



High-Speed Coating of Primer Layer for Li-Ion Battery Electrodes by Using Slot-Die Coating

Ralf Diehm,* Marcus Müller, David Burger, Jana Kumberg, Sandro Spiegel, Werner Bauer, Philip Scharfer, and Wilhelm Schabel

A reduction of the inactive components can increase the energy density and reduce production cost of Li-ion batteries. But an effective reduction of the binder amount also negatively affects the adhesion of the electrode. Herein, slot-die coating of a primer layer for Li-ion anodes is investigated. It is shown that the use of a primer layer with only 0.3 g m^{-2} can increase the adhesive force by the factor of 5 as well as the cell performance for anodes with low binder content. The process limits for a stable, defect-free primer coating are investigated at coating speeds of up to 550 m min^{-1} . The limits coincide both for a setup without vacuum box and with vacuum box with theory-based equations. By using a vacuum box, the minimum wet film thickness can be reduced by half.

1. Introduction

Many research activities for Li-ion battery electrodes aim to combine high cell capacity with low production cost. This often involves increasing the ratio of active-to-inactive electrode materials. However, a reduction of inactive materials, such as binder and conductive additives, becomes inappropriate when it leads to an undue deterioration of the electrode properties. In particular, the adhesive forces as well as the ionic and electrical conductivity are important electrode properties, which must be preserved in electrode design and processing.^[1–6] To handle the insufficient adhesion problem at low binder content, some approaches use multilayer electrodes with binder and additive gradients.^[7–10] One approach, which is used in this work, is to apply a very thin primer layer to the current collector to significantly improve the

R. Diehm, D. Burger, J. Kumberg, S. Spiegel, Dr. P. Scharfer, Prof. W. Schabel
Institute of Thermal Process Engineering, Thin Film Technology
Karlsruhe Institute of Technology (KIT)
Karlsruhe 76131, Germany
E-mail: ralf.diehm@kit.edu

Dr. M. Müller, Dr. W. Bauer
Institute for Applied Materials – Energy Storage Systems (ESS)
Karlsruhe Institute of Technology (KIT)
Hermann-von-Helmholtz-Platz 1, Eggenstein-Leopoldshafen 76344,
Germany

The ORCID identification number(s) for the author(s) of this article can be found under <https://doi.org/10.1002/ente.202000259>.

© 2020 The Authors. Published by WILEY-VCH Verlag GmbH & Co. KGaA, Weinheim. This is an open access article under the terms of the Creative Commons Attribution License, which permits use, distribution and reproduction in any medium, provided the original work is properly cited.

DOI: 10.1002/ente.202000259

adhesive force in combination with a low binder content in the active layer (see Figure 1). Several works have already addressed the properties of primers in battery electrodes. Doberdo et al. showed that a carbon coating protects the aluminum current collector foil from corrosion by using an aqueous binder system for lithium nickel manganese cobalt oxides (NMC) cathodes.^[11] Carbon-coated aluminum foil was also used in lithium sulfur batteries by Li et al. to improve the adhesion and the electrical conductivity leading to a better cell performance.^[12] For LiFePO_4 cathodes, the use of an aluminum current collector with

carbon primer enabled the reduction of additives in the active layer.^[13] With graphite anodes, it was shown that a graphene/polyvinylidene fluoride primer layer enhanced adhesion, conductivity, and cell performance.^[14] Nevertheless, the application of a primer layer generates an economical advantage only if the additional layer is sufficiently thin and cheap to produce. Otherwise, the primer layer will offset the advantages of the binder reduction. In addition, the primer layer should be manufactured at such low cost that the additional step is not relevant for the total production expense. This implicates that the electrodes, in particularly the primary layer, have to be manufactured with preferably high production throughput.^[15,16] Another cost-benefit arises from the application of aqueous slurry formulations due to lower material and postprocessing expenditures.

In this work, anodes with low binder content and good processability will be presented by using an electrode design with high-speed processed carbon primer layer. As very thin layers have to be produced at high production speeds, the number of applicable coating processes is limited. In this work, a modified slot casting process is explicitly investigated, which is similarly used in the production of battery electrodes. To reduce the minimum wet film thickness, a vacuum box is used. The limits compared with state-of-the-art slot-die coating without vacuum box are revealed.

2. Results and Discussion

In this study, the application of a very thin primer layer on a copper foil for Li-ion battery anodes via high-speed slot-die coating is investigated. The purpose of this thin primer layer is the improvement of electrode adhesion and reduction of binder content. This should reduce the total binder content of the electrode and improve the electrode performance.



Figure 1. Structure of an electrode with primer layer between active layer and current collector to improve the properties of the electrode.

2.1. Primer Formulation

A water-based formulation was developed, consisting of equal parts of carboxymethyl cellulose (CMC), styrene-butadiene rubber (SBR), and carbon black (CB), as shown in **Table 1**. CMC acts as a dispersant and film former, SBR as the main binder, and CB as conductive additive with a ratio of 1:1:1.

Two reference anodes were selected to compare the properties of the primer layer with regard to adhesion and cycle stability. One is an anode layer with a higher binder content, which corresponds to 93 wt% active material and sufficient adhesive force for the cell processing. The second anode has a strongly reduced binder content and 97 wt% active material. To increase the adhesion of the electrode with low binder, a primer was applied to the copper foil. The primer with the formulation shown in **Table 1** is applied with an area loading in the dry film of 0.3 g m^{-2} . This results in a total percentage of active material in the electrode of 96.5 wt%.

2.2. Microstructure

SEM images of top view and cross section of the electrode are shown in **Figure 2**. The primer layer is not deposited as a homogeneous thin film, but a regular accumulation of small and big particles of conductive CB and binder domains. The primer layer appears to form large contact regions between the film and the graphite layer, which are not present without primer.

2.3. Adhesion and Conductivity

A property that is directly influenced by the contact surface is the adhesion. Adhesion of the active layer on the substrate is an important parameter for the properties of the battery. The layer must not delaminate from the electrode during further assembling and cycling of the battery cells. The adhesive force required for industrial production depends on the respective production

Table 1. Compositions of the used slurries.

ID	Graphite [wt%]	CB [wt%]	CMC [wt%]	SBR [wt%]
Primer layer	0	33.2	33.5	33.3
Low binder anode	97.0	1.0	1.0	1.0
High binder anode	93.0	1.4	1.9	3.7

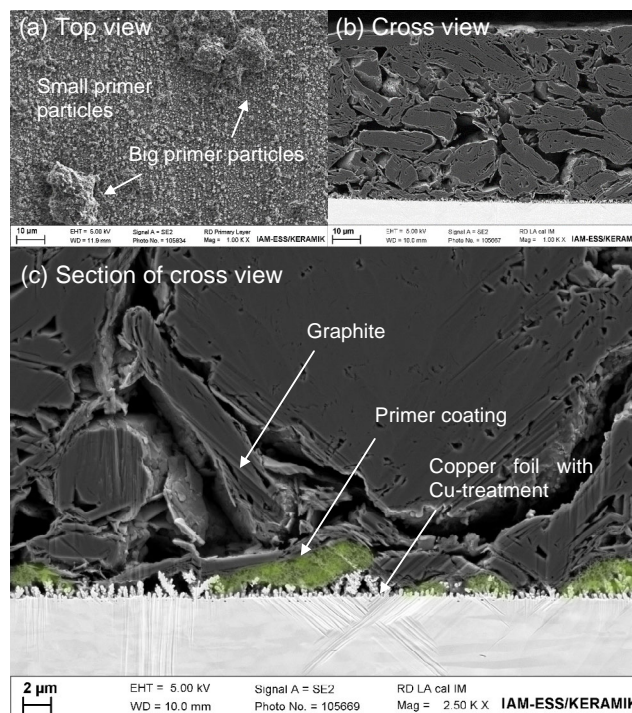


Figure 2. a) Top view of primer layer with big and small primer particles. b) Cross-profile of the electrode with primer and copper foil with Cu treatment. c) Section of the interface in higher resolution with primer coating between graphite and copper foil.

line and the individual cell geometry. For the cell production in pouch cells used by us, an adhesive force of more than 6 N m^{-1} is targeted. Here, a copper foil was used with copper treatment, which was supposed to improve the adhesive force even without primer layer. The resulting adhesion of the electrodes produced is shown in **Figure 3**.

The adhesion of the anode with low binder content is 1.5 N cm^{-1} . As expected, this is much lower than the 9.7 N cm^{-1} of the anode with high binder content. Due to the low adhesive force, it is difficult to process the electrodes with low binder

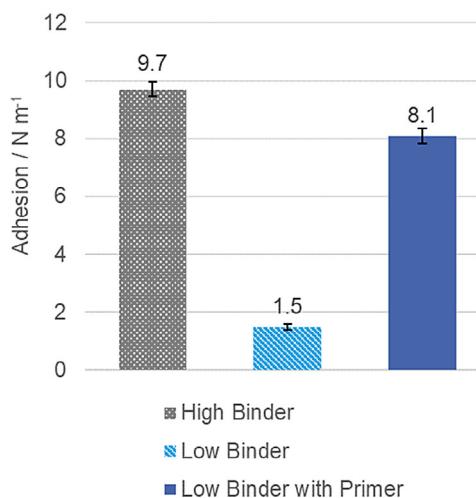


Figure 3. Adhesive force for the produced graphite anodes.

content into cells by hand. By using the primer layer, the adhesion is increased from 1.5 to 8.1 N m⁻¹ which allows processing similar to the electrode with high binder content. The electrodes with primer can therefore be processed similarly to the electrodes with high binder content. The addition of a primer layer reduces the proportion of active material in the electrode from 97.0 to 96.5 wt%. This is a very small loss of energy density in relation to the improvement of adhesion. With all three configurations, adhesion fracture mainly occurs between substrate and electrode coating or between substrate and primer coating, with small residues of coatings on the substrate.

The influence of the primer on the electrical conductivity within the graphite network was investigated with transmission conductivities (see Figure 4).

Reference electrodes with high binder content show the lowest conductivity with 3.9 S m⁻¹. The electrodes with low binder content have a higher conductivity of 4.9 S m⁻¹ compared with the reference. The highest conductivity is measured at 5.8 S m⁻¹ for the combination of low binder and primer.

The lowest conductivity of the high binder electrode can be attributed to the high binder content of 5.6% and the comparatively low conductive CB content of 1.4%. This results in less contact points between the graphite particles and the current collector. In the comparison of the two configurations with low binder content, the primer seems to improve the conductivity due to the high number of conductive CB particles on the surface of the collector foil (see Figure 2).

2.4. Electrochemical Performance

To measure the performance of the electrodes, full cells were produced in pouch format with NMC622 as described in Section 4. The results of the rate capability test and the cycling test are shown in Figure 5.

The initial discharge capacity of the reference with high binder, determined from the formation cycles at C/20, is 169 mAh g⁻¹, that with low binder is 158 mAh g⁻¹, and that with low binder and primer is 156 mAh g⁻¹. The difference in the initial capacity could be due to the larger surface area not covered

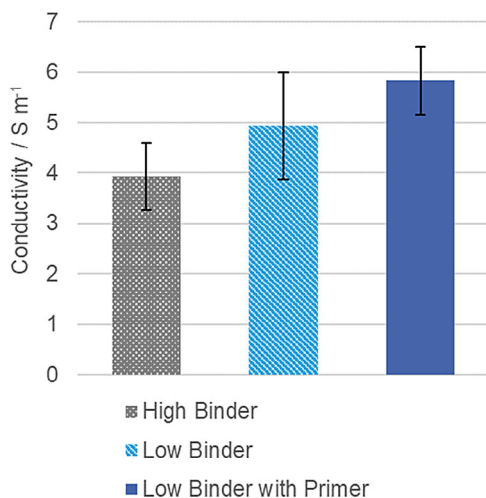


Figure 4. Electrical conductivity of the anodes.

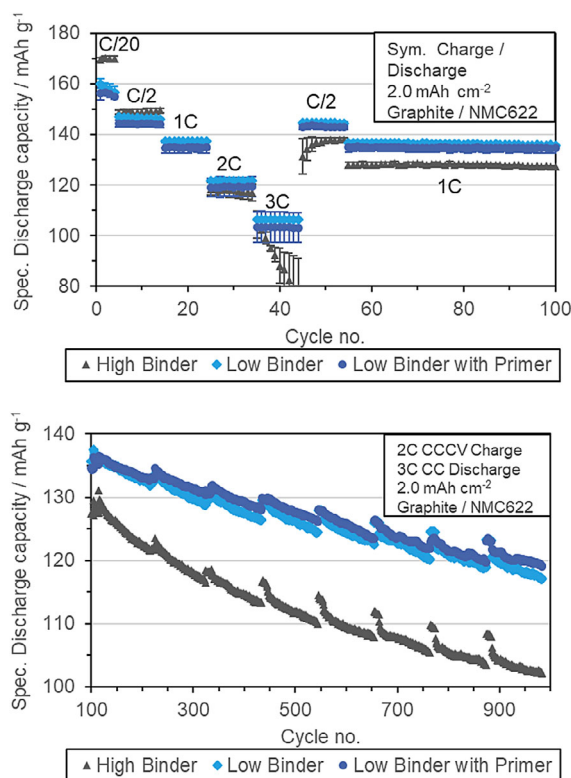


Figure 5. Rate capability test with CC (top) and aging test with 2C CCCV/3C CC cycles (bottom). NMC622 is used for the cathode with a capacity of 2.0 mAh cm⁻². After each 100 cycles of the aging test, 10 cycles were performed at 1C CC for comparison with the rate capability test.

with binder of the low binder anodes, which is available for solid-electrolyte interphase (SEI) formation and uses lithium from cathode. The charge and discharge curves are shown in Figure 6 for the first cycle. At low C rates, the low Li⁺ diffusion through the binder surfaces on the active particles is not limiting, which results in higher usable capacity due to less Li⁺ loss during SEI formation. Up to 1C, the capacities of the electrodes with low binder are similar to those with high binder. At high C rates of 2C and 3C, on the contrary, electrodes with low binder content show a significant higher usable capacity. The cells without

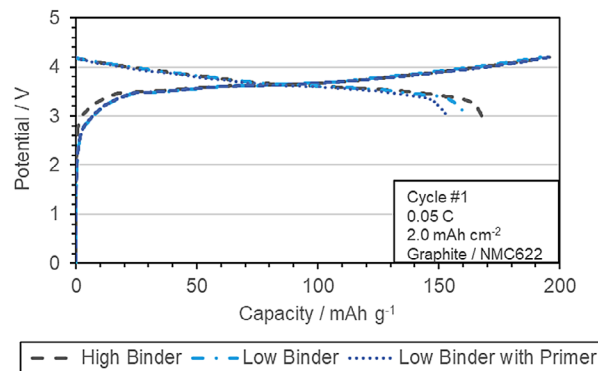


Figure 6. Cell potential over capacity for the first cycle at 0.05 C.

primer always have a slightly higher capacity than those with primer. Here, the advantage of the lower binder quantity on the particle surface outweighs the Li⁺ loss during SEI formation and leads to better performance. At 3C we observe a reduction of the capacity of the reference electrode with high binder content, which regenerates in the following C/2 cycles. Due to the hindrance of the Li⁺ diffusion by higher binder enrichment in the pores, lithium plating may occur on the surface at high charging currents. The charging rate for the aging test was therefore limited to 2C. In the aging test with 2C/3C CCCV, the degradation of the capacity of the electrodes with low binder is significantly lower than in the reference. This results in a significantly higher capacity of 126 mAh g⁻¹ for low binder at cycle 500 compared with 111 mAh g⁻¹ for the high binder reference. The low binder electrode with primer shows lower degradation than without primer. From cycle 120, this electrode has the highest residual capacity. The reason for the improvement at higher cycle numbers could be the better adhesion between the active material and the collector foil, which could lead to less detachment of active material due to volume expansion during cycling.

In summary, the use of a primer layer can reduce the inactive components of the electrode such as binders and conductive additives while maintaining the same mechanical strength of the electrode. This leads to better capacities at high C rates of 2C and 3C as well as significantly lower aging at 2C/3C CCCV.

2.5. Coating Stability and Upscaling

For industrial-scale implementation, this primer layer must be applied to the film at high speed and at low cost. For this, the stability limit of the coating process must be predicted. Especially with the production of very thin coatings, there are two limiting failure criteria for the low thickness limit of slot-die coating.^[17] These are air entrainment as instability of the moving contact line on the upstream side and low-flow as instability of the meniscus at the downstream side. Both limits are shown in **Figure 7**.

For determination of the process windows, the same primer slurry was used as for the electrode characterization. The materials were mixed with water as solvent as described in Section 4. The solids content of the coating slurry was 2.5 wt%. The slurry shows a strong shear-thinning behavior, as shown in **Figure 8**.

At low shear rates below 1 s⁻¹ the viscosity is higher than 1 Pa s, whereas at higher shear rates the viscosity decreases to less than 0.01 Pa s. The shear rates in the coating bead are between 1515 and 75 758 s⁻¹ in the investigated speed range

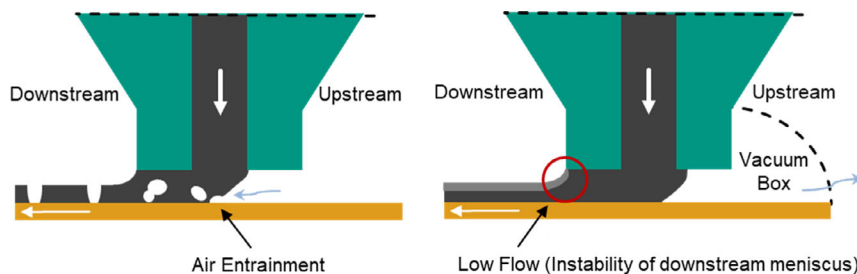


Figure 7. Failure mechanisms of slot-die coating. Air entrainment: Air bubbles are introduced into the film via the upstream meniscus (left). Low-flow: Instability of the downstream meniscus causes film thickness variation (right).

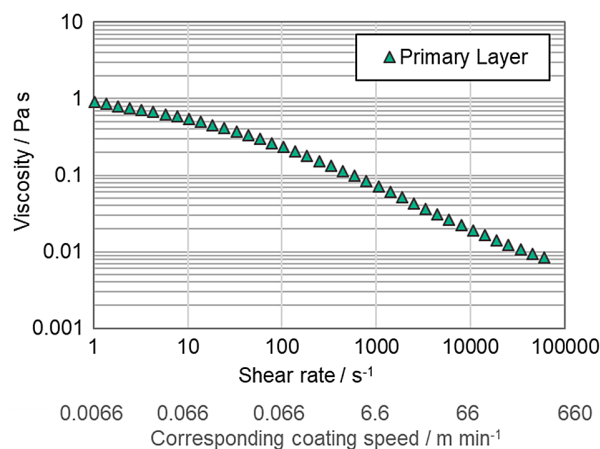


Figure 8. Viscosity of the primer slurry as a function of the applied shear rate. The second X-axis shows the corresponding coating speeds for this setup.

from 10 to 550 m min⁻¹. A power-law approach in the relevant range from 1000 to 100 000 s⁻¹ was used to describe the rheological behavior, as shown in Equation (1).

$$\mu_{\text{eff}} = K \left(\frac{\partial u}{\partial y} \right)^{n-1} \quad (1)$$

For the primer slurry, the flow consistency index K is 2.890 Pa s ^{n} and the flow behavior index n is 0.462. The surface tension of the primer slurry σ is 0.06938 N m⁻¹ (measured with Krüss, EasyDrop DSA20).

For the stable coating window, the limit that occurs at higher wet film thicknesses is relevant. When coating without vacuum box, coating defects occur that indicate air entrainment as the failure mechanism. To compare the experimental limits with theoretical limits, reference is made to a simulation based on the work of Ruschak, Higgins and Scriven, Durst, and Schmitt resulting in the following formula.^[8,18–20]

$$\Delta p_{\text{VAC}} = 1.34 \cdot \left(\frac{\kappa \cdot u_{\text{web}}^n}{\sigma \cdot h_G^{(n-1)}} \right)^{\frac{2}{3}} \cdot \frac{\sigma}{h_{\text{wet}}} + l_{\text{downstream}} \cdot \kappa \cdot \left(\frac{(n+1)(2n+1)}{n} \right)^n \cdot \frac{(h_G - 2 \cdot h_{\text{wet}})^n}{h_G^{(2n+1)}} \cdot u_{\text{web}}^n - \frac{2 \cdot \sigma}{h_G} \quad (2)$$

As no vacuum is applied without using the vacuum box, the pressure difference Δp_{VAC} is set to zero in this case.

$$\Delta p_{VAC} \stackrel{!}{=} 0 \quad (3)$$

The equation was iteratively solved to determine the minimum wet film thickness $h_{wet,min}$. **Figure 9** shows the experimental limits for the coating without vacuum box and the corresponding limit by the simulation. Coating defects occur at process points below the minimum wet film thickness. The characteristic coating defect of air entrainment with alternating coating as stripes perpendicular to the coating direction can be clearly observed.

The experimental limit values increase with increasing speed from $38.6 \mu\text{m}$ at 10 m min^{-1} to about $55 \mu\text{m}$ at higher coating speeds than 50 m min^{-1} . The experimental values remain at this value and do not increase any further. The simulation also shows an increase in the minimum wet film thickness with increasing speed up to 50 m min^{-1} . The limit approaches an asymptote at half the gap width between the slot caster and the substrate, which corresponds to $55 \mu\text{m}$ in this study. This results in a minimum basis weight of 1.5 g m^{-2} of the primer layer for the used formulation with 2.5 wt% solids at industrially relevant coating speed. At a speed of 200 m min^{-1} , the maximum possible pump flow rate of 1.8 L min^{-1} of the experimental setup is achieved.

One way to reduce the minimum wet film thickness even at high speeds is to apply a negative differential pressure to the upstream side of the slot-die. By this, air entrainment can be prevented and the stability of the downstream meniscus, known as the low-flow limit, determines the stable coating window. The low-flow limit can be approximated with the following formula^[18,19,21]

$$h_{wft,low-flow} = h_g \cdot \left(2 \cdot \left(\frac{\kappa \cdot u_{web}^n}{0.65 \cdot \sigma \cdot h_g^{n-1}} \right)^{-\frac{2}{3}} + 1 \right)^{-1} \quad (4)$$

The coating window with stabilization of the meniscus by the vacuum box is shown in **Figure 10**. For the first three experimental values at $10, 50, \text{ and } 100 \text{ m min}^{-1}$, the minimum wet film thickness increases from 18.5 up to $34.2 \mu\text{m}$. The values are slightly above the calculated low-flow limit, but they follow the same shape. After the increase to a maximum, a decrease in the minimum wet film thickness at higher speeds is observed. At 200 m min^{-1} at least $28.4 \mu\text{m}$ wet film thickness is required and at 550 m min^{-1} only $17.9 \mu\text{m}$ wet film thickness is required, which corresponds to a primer area weight of only 0.3 g m^{-2} . Higher coating speeds and thus high volume flow seem to cause a stabilization of the liquid flow. The experimental values over 200 m min^{-1} can be well described with an exponential approach of the following form^[22]

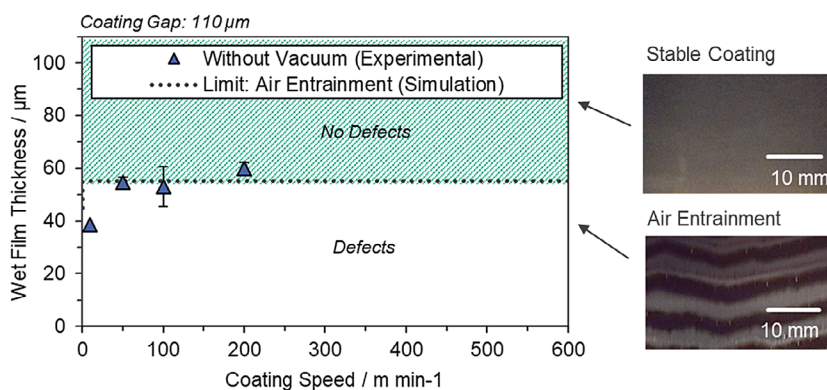


Figure 9. Limit of coating window without vacuum chamber and the resulting coating pattern for stable coating and coating defects.

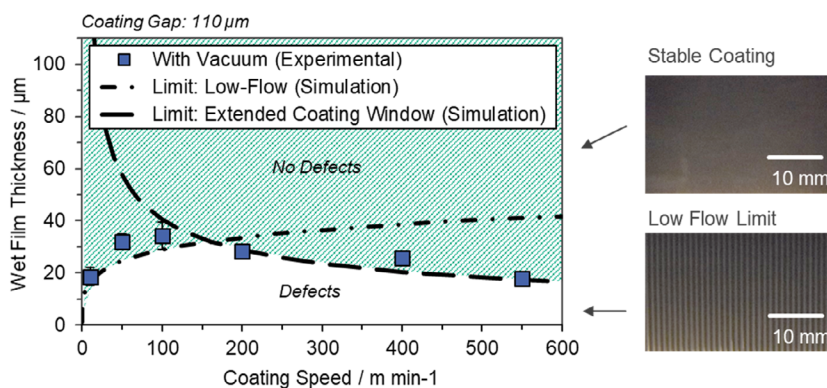


Figure 10. Coating window with vacuum box. Gap = $110 \mu\text{m}$. In addition to the experimental points, the simulated limits for low-flow and extended coating window are plotted.

Table 2. Minimum wet film thickness for different coating speeds with and without vacuum box and a coating gap of 110 μm .

Coating speed [m min^{-1}]	Minimum wet film thickness		Difference [μm]
	Without vacuum [μm]	With vacuum [μm]	
10	38.6 \pm N/A	18.5 \pm 3.5	-20.1
50	54.8 \pm 2.0	32.0 \pm 2.8	-22.8
100	53.1 \pm 7.6	34.2 \pm 5.2	-18.9
200	60.0 \pm 2.2	28.4 \pm 0.4	-31.6
400	N/A	25.8 \pm 2.2	-
550	N/A	17.9 \pm N/A	-

$$h_{\text{wft,ecw}} = \kappa_{\text{ecw}} \cdot u_{\text{web}}^{-\frac{1}{2}} \quad (5)$$

A good agreement of all measured values is found with

$$\kappa_{\text{ecw}} = 52.4 \mu\text{m} \cdot (\text{m} \cdot \text{min}^{-1})^{-\frac{1}{2}} \quad (6)$$

The minimum wet film thickness when using a vacuum box can thus be described as a combination of the formulas (4) for low-flow limit and (5) for the limit at higher speeds. Compared with the results without vacuum box, the minimum wet film thickness can be roughly halved by using a vacuum box. The differences are shown in Table 2.

Based on these results, stable coating parameters can be predicted and time can be saved in setting up the coatings.

3. Conclusion

In this work, high-speed slot-die coating of a primer layer for Li-ion battery electrodes was investigated. For this purpose, a water-based formulation was applied consisting of equal parts of CMC, SBR, and CB. It was shown that very thin primer layer films can be produced by slot-die coating. A process window up to 550 m min^{-1} web speed has been set up. For coating without support of a vacuum box, air entrainment was identified as the relevant defect mechanism. This results in a minimum wet film thickness at higher web speeds, which corresponds to about half the application gap as simulated. For coating with vacuum box, about half the minimum wet film thickness was achieved compared with the coating without vacuum box. Increasing the web speed, the minimum wet film thickness decreases again to 18 μm at 550 m min^{-1} . This was explained and described using the approach of an extended coating window.

Based on this, electrodes with primer layers of 0.3 g m^{-2} were produced and characterized using two different anode formulations with high and low binder content. The proportion of active material was increased from 93 wt% for the high binder reference electrode to 96.5 wt% for the low binder electrode with primer layer. The capacity of electrodes with low binder content is significantly higher than if using a high binder content and should therefore be preferred. The low adhesive force of the formulation with low binder content was increased with a primer layer by the factor of 5 from 1.5 to 8.1 N m^{-1} , which leads to similar processing capabilities as for the electrode with high binder

content. It was shown that the use of primer layers is a suitable and scalable way to improve the properties of the electrode. High-speed slot-die coating has been proven to be a suitable way to produce thin primer layer of just a few 100 nm at high production speed.

The results refer to the tested formulation for the primer layer. A differently optimized formulation with regard to composition and particle size could achieve even better results in other applications. The drying rate was kept constant at a high level of 1.5 $\text{g cm}^{-2} \text{s}^{-1}$ which results in a drying time of only 53 s for the electrode. Due to the lower binder formulation in combination with the primer layer, a further increase in drying speed might be possible in the future without excessive limitation in performance. With the significantly thinner primer layer, we expect a possible drying time of significantly less than the 7.3 s used, as there should be fewer problems with binder migration due to the layer thickness at higher drying rates. The web handling of sensitive substrates at very high speeds is demanding and needs to be investigated in this case.

4. Experimental Section

Slurry Materials and Preparation: The slurry for the primer layer was mixed using a dissolver (Dispermat SN-10, VMA-Getzmann/Germany). CB (Imerys C65) powder was deagglomerated in a dry mixing step at 1350 rpm for 10 min. After dry mixing, a premixed 2 wt% CMC (Sunrose, Nippon paper industries) solution was added together with water to adjust the desired dilution of 2.5 wt% in the formulation. The mixing was continued for 30 min at 1130 rpm. The binder SBR (Zeon) was stirred in at the end for 10 min at a low speed of 200 rpm.

The anode slurry was prepared by dry mixing of the solids, graphite, and CB. The binder and dispersing agent CMC were premixed in water and gradually added to the solids in three steps. A kneading device (Inoue Mfg, Japan) was used for the mixing steps with dispersing time of 10, 30, and 120 min after each dilution step. The solids content was set to 43 wt% after dilution for high binder anode and 50 wt% for low binder anode. Subsequently, SBR dispersion was added. Two different anode formulations were used for the active layer. The high binder anode with 93 wt% active material consists of 93 wt% graphite, 1.4 wt% CB, 1.9 wt% CMC, and 3.7 wt% SBR binder. The low binder anode with 97 wt% active material consists of 97 wt% graphite, and 1 wt% CB, CMC, and SBR binder, respectively.

The viscosity was measured by a rotation viscometer in plate-plate setup with 25 mm diameter (Anton Paar, Germany) from 0.01 to 10 000 s^{-1} . The return path of the hysteresis measurement was evaluated to get a constant shear history.

Process Window Characterization: The tests were conducted with a development coater on which the slurry was applied directly onto a chrome-plated high-precision roller (see Figure 11). To ensure that the existing dryer length and the resulting maximum web speed do not limit the tests, a continuous coating without substrate was used. The slurry was removed from the roller after coating and analysis. The speed was varied between 10 and 550 m min^{-1} . The slot between the slot-die plates was adjusted to 200 μm by means of a shim. The distance between the slot-die outlet lips and the rotating roller was held constant 110 \pm 1.5 μm .

Anode Coating, Drying, and Calendering: The coating of the battery electrodes was conducted on a batch electrode coater. The copper foil used as current collector (Schlenk, 13 μm thickness, Cu-Treatment) was surface modified by the manufacturer with a copper treatment. The treatment was intended to improve the adhesion with low binder anodes. The foil was applied to a temperature-controlled plate. Subsequent to coating, the wet film was moved instantly below an impingement dryer. The plate moved cyclically back and forth to obtain homogeneous drying conditions, until the electrode was dried. The dryer

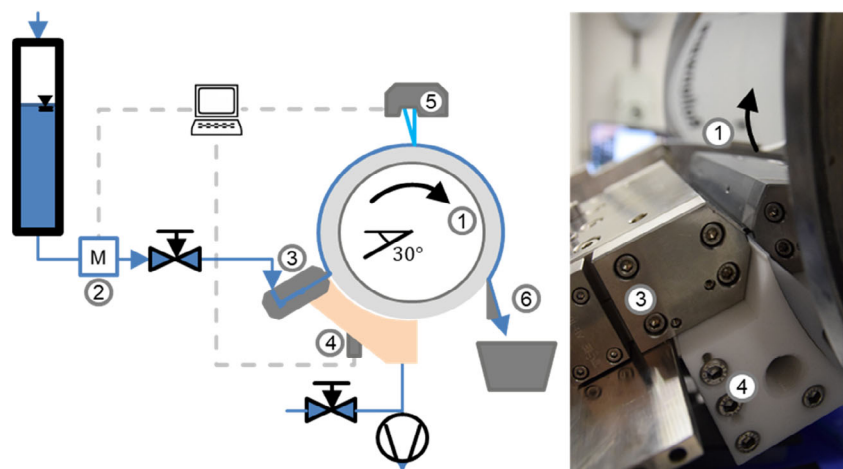


Figure 11. Experimental setup of development coater with rotating high-precision roller (1), fluid delivery system (2), slot-die (3), vacuum box (4), wet film thickness measurement systems (5), and blade to remove the coating (6).

consisted of an array of 20 slot nozzles. The area loading was set in each case so that an equal area capacity of $2.2 \pm 0.7 \text{ mAh cm}^{-2}$ was achieved. As the drying time had a direct influence on the processing costs, a constant high drying rate of $1.5 \text{ g m}^{-2} \text{ s}^{-1}$ was used, which corresponds to a short drying time of 53 s for the anode layer and 7.3 s for the primer layer. The dew point of the inlet air was $3.1 \text{ }^\circ\text{C}$. The heat transfer coefficient of the dryer was constant at $35 \text{ W m}^{-2} \text{ K}^{-1}$. The dried electrode layers were finally calendered to a porosity of 45% with heated rolls at $50 \text{ }^\circ\text{C}$ (Saueressig GKL 200).

Methods for Layer Characterization: A 90° peel test was used for adhesion characterization (AMETEK LS1 with 10 N load cell). The electrode was cut into 30 mm strips with $>40 \text{ mm}$ length and applied with the coating side to an adhesive stripe. The current collector foil was then pulled off at an angle of 90° with a constant velocity of 50 mm min^{-1} . The required pull-off force was measured and divided by the sample width to get the adhesive line force.

A self-constructed measuring device was used for conductivity characterization. The sample was placed between two copper stamps of 40 mm diameter and a force of 17.8 N. An E3633A from Agilent Technologies was used for the current source. The electrical resistance was determined by means of a four-wire measurement with a Keyence 2700 multimeter and converted to the electrical conductivity.

Cell Preparation and Test: The electrodes were built into full cells in pouch format (approximately $50 \times 60 \text{ mm}^2$, three full cells each electrode) and electrochemically examined. For the cathode, a standard electrode made of NMC 622 with a loading of 11.5 mg cm^{-2} and a capacity of 2.0 mAh cm^{-2} . A ceramic-coated nonwoven separator was used (SEPARION S240P30). The electrolyte was a mixture of EC:DMC 1:1 with 1M LiPF₄ and 3 wt% VC.

The rate capability was tested in constant current mode with identical charging and discharging rates. After two formation cycles with C/20, the C rate was varied between C/2 and 3C. To investigate the long-term stability, cells were charged with 2C, followed by a constant voltage step at 4.2 V until the current dropped to a value corresponding to C/20, followed by discharging with 3C. After 100 cycles, 10 cycles with 1C charging and 1C discharging were performed. This procedure was repeated until 1200 cycles in total had been achieved.

Acknowledgements

The authors thank Dr. Amalia Wagner for her support in cell making and electrochemical characterization and TSE Troller AG for the technical support.

Conflict of Interest

The authors declare no conflict of interest.

Keywords

carbon coating, coating window, Li-ions, primer layers, slot-die coating, vacuum box

Received: March 20, 2020

Revised: May 8, 2020

Published online:

- [1] M. Yoshio, R. Brodd, A. Kozawa, *Lithium-Ion Batteries*, Springer, Berlin/New York **2009**.
- [2] H. Bockholt, M. Indrikova, A. Netz, F. Golks, A. Kwade, *J. Power Sources* **2016**, *325*, 140.
- [3] S. Jaiser, J. Kumberg, J. Klaver, J. L. Urai, W. Schabel, J. Schmatz, P. Scharfer, *J. Power Sources* **2017**, *345*, 97.
- [4] C. C. Li, Y. W. Wang, *J. Electrochem. Soc.* **2011**, *158*, 1361.
- [5] J. Kumberg, M. Müller, R. Diehm, S. Spiegel, C. Wachsmann, W. Bauer, P. Scharfer, W. Schabel, *Energy Technol.* **2019**, *1900126*, 1.
- [6] S. Lim, K. H. Ahn, M. Yamamura, *Langmuir* **2013**, *29*, 8233.
- [7] D. Liu, L. C. Chen, T. J. Liu, W. B. Chu, C. Tiu, *Energy Technol.* **2017**, *5*, 1235.
- [8] M. Schmitt, S. Raupp, D. Wagner, P. Scharfer, W. Schabel, *J. Coat. Technol. Res.* **2015**, *12*, 877.
- [9] L. C. Chen, D. Liu, T. J. Liu, C. Tiu, C. R. Yang, W. B. Chu, C. C. Wan, *J. Energy Storage* **2016**, *5*, 156.
- [10] R. Diehm, J. Kumberg, C. Dörrer, M. Müller, W. Bauer, P. Scharfer, W. Schabel, *Energy Technol.* **2020**, *8*, 1901251.
- [11] I. Doberdò, N. Löffler, N. Laszczynski, D. Cericola, N. Penazzi, S. Bodoardo, G. T. Kim, S. Passerini, *J. Power Sources* **2014**, *248*, 1000.
- [12] T. Li, H. Bo, H. Cao, Y. Lai, Y. Liu, *Int. J. Electrochem. Sci.* **2017**, *12*, 3099.
- [13] C. Busson, M. A. Blin, P. Guichard, P. Soudan, O. Crosnier, D. Guyomard, B. Lestriez, *J. Power Sources* **2018**, *406*, 7.

- [14] S. Lee, E. S. Oh, *J. Power Sources* **2013**, 244, 721.
- [15] M. Schmitt, M. Baunach, L. Wengeler, K. Peters, P. Junges, P. Scharfer, W. Schabel, *Chem. Eng. Process. Process Intensif.* **2013**, 68, 32.
- [16] R. Diehm, J. Kumberg, P. Scharfer, W. Schabel, in *ISCST, AIMCAL*, Long Beach, CA, USA **2018**.
- [17] X. Ding, J. Liu, T. A. L. Harris, *AIChE J.* **2016**, 62, 2508.
- [18] K. J. Ruschak, *Chem. Eng. Sci.* **1976**, 31, 1057.
- [19] B. G. Higgins, L. E. Scriven, *Chem. Eng. Sci.* **1980**, 35, 673.
- [20] N. Dongari, R. Sambasivam, S. F. Durst, *Coat. Int.* **2007**, 40, 10.
- [21] O. J. Romero, W. J. Suszynski, L. E. Scriven, M. S. Carvalho, *J. Nonnewton. Fluid Mech.* **2004**, 118, 137.
- [22] M. S. Carvalho, H. S. Khashgi, *AIChE J.* **2000**, 46, 1907.